

Millennial- and centennial-scale droughts at the northern margin of the East Asian summer monsoon during the last deglaciation: Sedimentological evidence from Dali Lake

Jiawei Fan^{a,b,*}, Jule Xiao^{a,b,c}, Xiaoguang Qin^{a,b}

^a Key Laboratory of Cenozoic Geology and Environment, Institute of Geology and Geophysics, Chinese Academy of Sciences, Beijing 100029, China

^b Institutions of Earth Science, Chinese Academy of Sciences, Beijing 100029, China

^c College of Earth Sciences, University of Chinese Academy of Sciences, Beijing 100049, China

ARTICLE INFO

Keywords:

Bayesian age–depth model
Log-normal distribution
Grain-size components
Lake level
Aeolian activity
Northern China

ABSTRACT

The semi-arid areas at the northern margin of the East Asian summer monsoon (EASM) have experienced an increased frequency of drought in recent decades. However, it is unclear whether past monsoonal precipitation in the region were determined mainly by El Niño-Southern Oscillation (ENSO) variability or high-latitude cooling. In this study, we use a high-resolution grain-size dataset combined with a new Bayesian age–depth model of a sediment core from Dali Lake to analyze the occurrence of millennial- and centennial-scale droughts at the EASM margin during the interval of climatic warming during the last deglaciation. The polymodal grain-size distributions are partitioned using a log-normal distribution function fitting method. High percentages of the coarse components (C4 + C5 + C6) are recognized as proxy indicators of strong aeolian activities and low lake levels, and thus droughts in the region. The drought events indicated thereby are generally accompanied by decreases in regional temperature, catchment surface runoff and bio-productivity, on both millennial and centennial timescales. These results imply that the droughts at the EASM margin were caused by a significantly weakened EASM intensity. In addition, the droughts may be linked, within the age uncertainties, to the Heinrich 1 (H1) and Younger Dryas (YD) events on millennial timescales, and to the Older Dryas (OD) cold event on centennial timescales, implying strong high-latitude forcing. Given that these cold reversals over northern high latitudes were induced by the rapid input of glacial melt-water to the North Atlantic during the last deglaciation, it is possible that ongoing climatic warming, and the resulting high northern-latitude ice-sheet melting, may cause an increased incidence of drought in northern China.

1. Introduction

Water resources are crucial for socio-economic development at the modern northern margin of the East Asian summer monsoon (EASM), which has frequently suffered from droughts in recent decades (Ding et al., 2008). The EASM plays the major role in transporting heat and moisture from low to high latitudes (An, 2000), and therefore the issue of whether EASM circulation will strengthen or weaken in the course of continued global warming is of critical importance.

Recent studies have suggested that there were substantial differences in regional hydro-climatic conditions across monsoonal China during the Holocene (Xiao et al., 2004; Chen et al., 2015a; Cheng et al., 2016; Wen et al., 2017; Fan et al., 2016, 2018a). In southern China, north-south migrations of the inter-tropical convergence zone (ITCZ),

accompanied by variations in the El Niño-Southern Oscillation (ENSO), and the strength and position of the West Pacific subtropical high (WPSH), have been considered key factors influencing variations in monsoonal precipitation (Yan et al., 2011; Xie et al., 2013; Chen et al., 2015b; Rao et al., 2016; Lu et al., 2018). The dominant influence of the migration of the ITCZ would have resulted in increased monsoonal precipitation in southern China during the early to middle Holocene (Wang et al., 2005; Wang et al., 2016; Lu et al., 2018); while the increased amplitude and frequency of ENSO would have forced the strengthened WPSH to move southwestwards, leading to increased monsoonal precipitation in the middle Yangtze River, on the frontier of the WPSH, during the late Holocene (Rao et al., 2016; Huang et al., 2018; Lu et al., 2018). However, in northern China monsoonal precipitation was weak during the early Holocene due to the remnant ice

* Corresponding author at: Key Laboratory of Cenozoic Geology and Environment, Institute of Geology and Geophysics, Chinese Academy of Sciences, Beijing 100029, China.

E-mail address: jwfan@mail.iggcas.ac.cn (J. Fan).

<https://doi.org/10.1016/j.palaeo.2018.11.001>

Received 21 May 2018; Received in revised form 26 October 2018; Accepted 1 November 2018

Available online 07 November 2018

0031-0182/ © 2018 Elsevier B.V. All rights reserved.

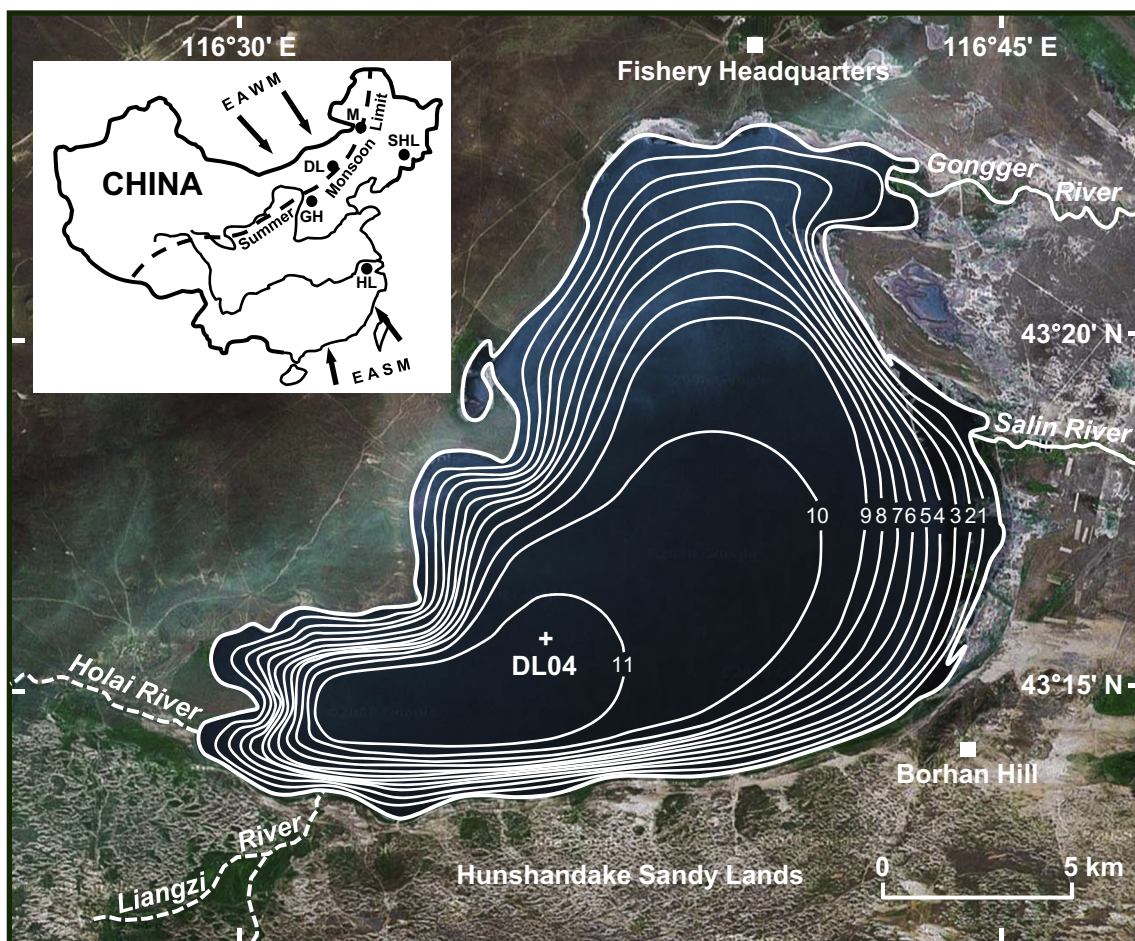


Fig. 1. Map of Dali Lake (from <http://maps.google.com>) showing the location of sediment core DL04 (cross). The bathymetric survey of the lake was conducted in June 2002 using a FE-606 Furuno Echo Sounder (contours in m). The inset map shows the locations of Dali Lake (DL; 43°15' N, 116°36' E), Sihailongwan Lake (SHL; 42°17' N, 126°36' E), Moon Lake (M; 47°30' N, 120°52' E), Gonghai Lake (GH; 38°54' N, 112°14' E) and Hulu Cave (HL; 32°30' N, 119°10' E) in China (solid circles) and the modern northern limit of the East Asian summer monsoon defined by the 400-mm isohyet of mean annual precipitation (Xiao et al., 2004).

sheets and the resulting low sea levels; and significantly increased during the middle Holocene, in response to the rapid retreat of ice sheets and rising sea levels; in addition, monsoonal precipitation decreased with decreasing western tropical sea surface temperature (WPSST) and increasing ENSO variability during the late Holocene (Xiao et al., 2004; Chen et al., 2015a; Wen et al., 2017; Fan et al., 2018a; Sun et al., 2018a).

Similar mechanisms have been applied to interpret climatic events during the last deglaciation (Hong et al., 2010; Stebich et al., 2011; Huang et al., 2012; Park et al., 2014; Russell et al., 2014; Zhou et al., 2016). For example, the lipid-based paleohydrological record from Dajiuhe peatland in the middle reaches of the Yangtze River indicates increased precipitation at the interval corresponding to the Younger Dryas (YD) period, in response to the southward migration of the WPSH (Huang et al., 2012); however, the pollen record from Gonghai Lake (GH) in northern China indicates decreased precipitation responding to significant cooling in northern high latitudes (Chen et al., 2015a). It has been argued that ENSO variability could have played the dominant role in increasing the monsoonal precipitation in northeast China at the interval corresponding to the YD period (Hong et al., 2010); however, others have demonstrated that high-latitude forcing may have dominated climatic change in southern China during the same period (Chu et al., 2017; Zhong et al., 2018). Thus, there is little consensus about whether ENSO variability or high-latitude cooling dominated monsoonal precipitation in China during the last deglaciation.

Recent climate model simulations have suggested that high-latitude

cooling associated with Arctic ice expansion and reduction in Atlantic Meridional Overturning Circulation (AMOC) could lower the temperature of northwesterly and westerly winds over East Asia during the last deglaciation, deliver cold air masses to northern China, and vice versa (Zheng et al., 2017). Geological records based on carbonate and organic geochemistry of a sediment core from Dali Lake at the modern northern margin of the EASM have provided an overall description of millennial climatic change during the last deglaciation (Fan et al., 2017, 2018b). The results indicated a generally warm and wet phase from 15–12.7 cal kyr BP, corresponding to the Bølling-Allerød (BA) warm period occurring in the North Atlantic and Northern European region; and a generally cold and dry phase from 12.7–11.5 cal kyr BP, corresponding to the Younger Dryas (YD) cold reversal. This correspondence provided evidence for atmospheric tele-connections with high latitudes on millennial timescales (Fan et al., 2017, 2018b). However, there are still some issues on the interpretation of climatic proxies of carbonate and organic geochemistry. For example, the precipitation of carbonate in Dali Lake was affected both by temperature and hydrological balance of lake water, how to separate the above two distinct factors (Fan et al., 2018b); the accumulation of lacustrine organic matter was controlled both by hydrological and ecological status in the lake catchment, which factor was more important (Fan et al., 2017). These issues may have hidden some important climate information during the last deglaciation, on millennial and especially on centennial timescales. Therefore independent climatic proxy related to a single environmental variable is needed to provide more insights into the changes in each climatic factor

and its possible driving mechanism.

Here, we present a new high-resolution (10–21 yr) record of climatic change from the modern northern margin of the EASM during the last deglaciation. The record is based on fitting log-normal distribution functions (Qin et al., 2005; Xiao et al., 2012) to grain-size data from 413 samples from Dali Lake. The aim of this study is to investigate the potential linkages between droughts at the monsoonal margin in northern China and cold climatic reversals at high northern latitudes, such as the Heinrich 1 (H1) and YD events on millennial timescales, and the Older Dryas (OD) event on centennial timescales, and to provide possible insights into how the EASM may respond to ongoing global warming and the associated ice-sheet melting at high northern latitudes.

2. Study site and regional setting

Dali Lake (43°13′–43°23′ N, 116°29′–116°45′ E) is an inland closed-basin lake in the central-eastern Inner Mongolian Plateau (Fig. 1). The lake has an area of 238 km², a maximum water depth of 11 m and an elevation of 1226 m above sea level. The lake basin was formed by tectonic subsidence in the Pliocene to Pleistocene (Li, 1993). The topography of the basin is like a pan, with steep slopes in the west, south and east and relatively flat terrain in the center and north (Fig. 1). The lake is located at the northern margin of the E–W trending Hushandake Sandy Lands. Hills of basaltic rocks surround the lake to the north and west, and lacustrine plains are present along the eastern shore (Li, 1993). Two permanent rivers, the Gongger and Salin Rivers, enter the lake from the northeast and two intermittent streams, the Holai and Liangzi Rivers, enter from the southwest (Fig. 1).

Dali Lake is located at the northern margin of the EASM (Fig. 1). The area has a mean annual temperature is 3.2 °C with a July average of 20.4 °C and a January average of –16.6 °C (Fan et al., 2016). Mean annual precipitation is 383 mm with ~70% of the annual precipitation falling in June–August (Fan et al., 2016). Mean annual evaporation reaches 1632 mm (Fan et al., 2016). The lake is ice-covered from early November to late April.

The modern natural vegetation of the Dali Lake basin is categorized as middle temperate steppe and is dominated by grasses (Compilatory Commission of Vegetation of China, 1980; Li, 1993). In the Hushandake Sandy Lands, low-growing xerophilous plants including *Polygonum divaricatum*, *Agriophyllum squarrosum* and *Artemisia desteroorum* are present, together with the shrubs *Salix gordevii*, *Ulmus pumila* and *Caragana sinica*. Forests consisting of *Larix gmelinii*, *Pinus tabulaeformis*, *Betula platyphylla*, *Populus davidiana* and *Quercus mongolica* are distributed on the western slopes of the Great Hinggan Mountains, where the Gongger River rises, together with shrubs and herbs growing beneath the canopy. Herbs including *Stipa grandis*, *Leymus chinensis* and *Cleistogenes squarrosa* are developed in the northern and western hilly lands and on the eastern lacustrine plains. There are few pastures scattered on the lacustrine plains.

3. Material and methods

3.1. Core DL04

The interval from 7.71–11.83 m of sediment core DL04, recovered from the depocenter of Dali Lake (43°15.68′ N, 116°36.26′ E) (Fig. 1), is used for the present study. The coring procedure is described in Xiao et al. (2008). The sediments consist of blackish-grey to greenish-grey, massive silt, and can be divided into four main sedimentary units (Fig. 2A), as follows: 1183–985 cm blackish-grey massive silt with greenish-grey bands at depths of 1183–1113 cm; 985–875 cm greyish-black massive silt; 875–789 cm blackish-grey massive silt; 789–770 cm greenish-grey massive silt with occasional blackish-grey bands. (Fan et al., 2018b).

3.2. Chronology

Eight bulk samples were collected from organic-rich horizons from the interval 7.71–11.83 m of core DL04 for accelerator mass spectrometry (AMS) ¹⁴C dating. All samples were measured with a Compact-AMS system (NEC Pelletron) by Paleo Labo Co., Ltd. (Japan). The reservoir effect of each horizon was corrected by subtracting the radiocarbon age of the uppermost 1 cm of core DL04 from the original radiocarbon dates (Fan et al., 2018b) (Table 1). The resulting ages were calibrated using the OxCal 4.2 age calibration program (Bronk Ramsey and Lee, 2013) with the IntCal13 calibration data (Reimer et al., 2013) (Table 1).

The age–depth model is based on a Bayesian Accumulation Model (Blaauw and Christen, 2011). The 7.71–11.83 m of core DL04 is divided into 83 vertical sections of 5 cm thickness each. Prior settings for the accumulation rates are prescribed by a gamma distribution with a mean of 20 yr/cm. The age of each sampled horizon at 95% confidence intervals is calculated for the 7.71–11.83 m of the core and then the weighted mean age is taken as the final age.

3.3. Grain-size analysis

The 7.71–11.83 m of core DL04 is sampled at 1-cm interval for grain-size analysis, yielding a total of 413 samples. The grain-size distributions of all samples are measured using a Malvern Mastersizer 2000 laser grain-size analyzer. Dried samples are pretreated with 30% H₂O₂ and 10% HCl in sequence to remove organic matter and carbonates, respectively, and then dispersed with 0.05 M (NaPO₃)₆ in an ultrasonic vibrator. The Mastersizer 2000 provides the volume percentage of each grain-size fraction at an interval of 0.166 Φ (Φ = –log₂ (D), where D is the grain diameter in mm). The relative error is < 2%. The grain-size frequency distributions of all samples are partitioned using the log-normal distribution function fitting method described in Qin et al. (2005) and Xiao et al. (2012).

4. Results

4.1. Age–depth model

The Bayesian modeling results show that the weighted mean ages of dated samples at the upper (799–798 cm) and lower (1150–1149 cm) horizons of the 7.71–11.83 m of core DL04 are 15,490 and 10,721 cal yr BP, respectively (Fig. 2B; Table 1). The dependence of the accumulation rate between neighboring depths was moderate after > 7500 iterations for the 83 vertical sections (Fig. 2B–E). The age–depth model produced by the Bayesian Accumulation Model shows that the 7.71–11.83 m of core DL04 spans the last deglaciation, from 16.2–10 cal kyr BP (Fig. 2B; Table 1). The 1-cm sampling interval yields a temporal resolution of 10–21 yr.

4.2. Characteristics of the grain-size components

Fittings of the lognormal distribution function show that the poly-modal grain-size distributions of the samples from Dali Lake are composed of three to six unimodal distributions representing three to six grain-size components (modes) (Fig. 3). These components are designated as C1 through C6 from fine to coarse modes, respectively (Fig. 3). As shown in Fig. 3C and Fig. 3D, the relatively separated modes are determined (for example, C3 and C4 in sample DL 1048 or C4 and C6 in sample DL 1168). To separate out two strongly overlapped components (for instance, C2 and C3 in samples DL 1048 and DL 1168), however, requires technical skills through trial-and-error fittings after careful observation. In this case, the fitting residual increases significantly if the minor component (C2 in samples DL 1048 and DL 1168) is ignored. Fitting experiments on 413 samples from 7.71–11.83 m of core DL04 yield the best fitting results from most of the samples with the squared

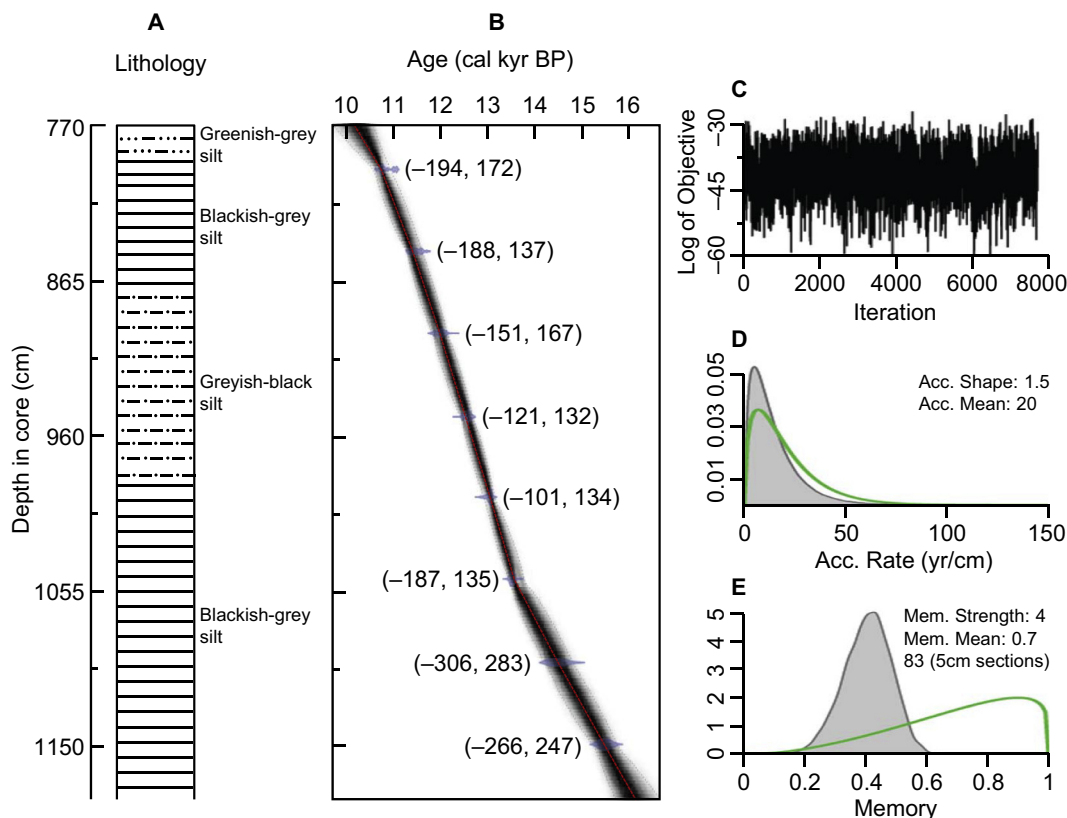


Fig. 2. Lithology and age–depth model of the interval 7.71–11.83 m of sediment core DL04. (A) Lithology of the interval 7.71–11.83 m of the core. (B) Calibrated ¹⁴C dates (blue: 2σ errors of 8 dated samples) and the age–depth model (darker grey shading indicates the more likely calendar ages; grey stippled lines show 95% confidence intervals; red curve shows the single ‘best’ model based on the weighted mean age for each depth; numbers in brackets indicate the ranges of uncertainties of 8 dated samples in the age–depth model). (C) Number of Markov Chain Monte Carlo (MCMC) iterations used to generate the grey-scale graphs. (D) Prior (green) and posterior (grey) distributions of the sediment accumulation rates (mean sediment accumulation rate is 20 yr/cm). (E) Prior (green) and posterior (grey) distributions of memory (dependence of the sediment accumulation rate between neighboring depths). (For interpretation of the references to color in this figure legend, the reader is referred to the web version of this article.)

Table 1
AMS radiocarbon dates of samples from the interval 7.71–11.83 m of core DL04.

Laboratory number ^a	Depth interval (cm)	Reservoir-corrected ¹⁴ C age ^b (¹⁴ C yr BP)	Calibrated ¹⁴ C age (2σ) ^b (cal yr BP)	Range of ¹⁴ C age ^c (cal yr BP)	Weighted mean ¹⁴ C age ^d (cal yr BP)
PLD-12470	799–798	9497 ± 39	10,654–10,869	10,549–10,915	10,721
PLD-12472	849–848	9992 ± 44	11,267–11,640	11,267–11,592	11,404
PLD-12474	899–898	10,243 ± 41	11,805–12,141	11,816–12,133	11,982
PLD-12477	950–949	10,578 ± 42	12,515–12,670	12,423–12,677	12,556
PLD-12478	999–998	11,158 ± 44	12,898–13,117	12,913–13,148	13,047
PLD-12480	1049–1048	11,686 ± 44	13,431–13,585	13,453–13,774	13,587
PLD-12483	1100–1099	12,404 ± 48	14,164–14,818	14,228–14,817	14,511
PLD-13857	1150–1149	12,964 ± 45	15,290–15,713	15,242–15,756	15,490

^a PLD: Paleo Labo Dating, laboratory code of Paleo Labo Co., Ltd., Japan.
^b The original data are cited from Fan et al. (2018b).
^c The range of ¹⁴C age is based on a Bayesian Accumulation Model.
^d The weighted mean ¹⁴C age is based on a Bayesian Accumulation Model.

sum of residual error < 4.

Grain-size data show that the respective modal size ranges of these six components C1 through C6 are 0.8–3.0, 2.2–7.5, 6.2–30.2, 41.6–172.8, 210.1–570.9 and 603.7–1568.1 μm (Fig. 4; Table 2), and the corresponding percentages range from 0.5–23.3%, 1.3–87.0%, 2.0–82.5%, 0.3–69.8%, 0.3–60.3% and 0.5–15.5% (Fig. 5; Table 2). Components C3 and C4 have their dominant modal sizes centered on 13.1 and 103.5 μm, respectively (Figs. 4 and 6). In addition, components C1–C3 are present in all 413 samples, while components C4–C6 exist only in 362, 125 and 32 samples, respectively (Fig. 5; Table 2). The component C4 generally accounts for > 10% in percentile when

both C2 and C3 are < 35% (Figs. 5 and 7). Finally, the components C5 and C6 appear in samples when C2 and C3 generally make up no > 20% in percentile (Figs. 5 and 7).

5. Discussion

5.1. Interpretation of grain-size components

Hydrological and meteorological observations suggest that the clastic sediments in Dali Lake are mainly derived from fluvial material transported during the summer season and from aeolian material

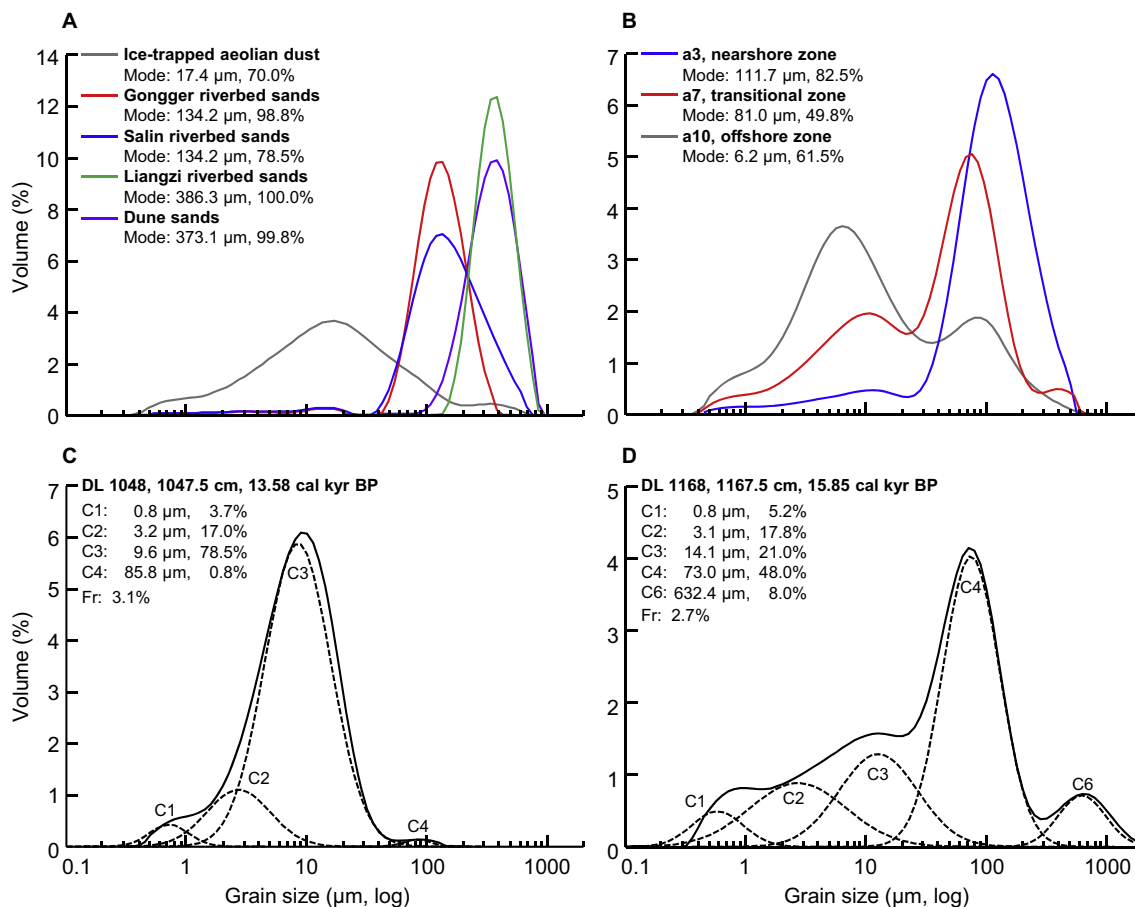


Fig. 3. (A) Frequency distribution curves of modern aeolian dust trapped on the ice in the depo-center of Dali Lake, modern riverbed sands deposited close to the mouths of the Gongger, Salin and Liangzi Rivers, and modern dune sands deposited close to the mouth of the Liangzi River. The dominant modal size and its percentage representation within each sample are shown. The original data are cited from Xiao et al. (2015). (B) Frequency distribution curves of three representative surface-sediment samples (a3, a7 and a10) from the nearshore, transitional and offshore zones of Dali Lake, respectively (Xiao et al., 2015). The dominant modal size and its percentage for each sample are shown. (C) and (D) Frequency distribution curves (solid lines) of two representative samples (DL 1048 and DL 1168) from the interval 7.71–11.83 m of core DL04; the depth and age of the two samples are shown following the sample number. Grain-size components (modes) can be recognized in the polymodal distributions (dashed lines), and are designated C1–C6 from fine to coarse modes. The sizes and percentages of each mode and the fitting residuals (Fr) of the two samples are shown.

transported by northwesterly and westerly winds during the dry and windy winter and spring (Li, 1993; Wang et al., 2002). Clastic materials from these sources are deposited on the lake floor after reworking by hydraulic processes in the lake basin (Håkanson and Jansson, 1983). In the Dali Lake catchment, the riverbed sands close to the mouths of the Gongger and Salin Rivers in the northeastern part of the lake have a dominant modal size of 134.2 μm ; the riverbed sands close to the mouth of the Liangzi River have a dominant modal size of 386.3 μm ; and dune sands to the southwest of the lake and ice-trapped aeolian dust have dominant modal sizes of 373.1 and 17.4 μm , respectively (Figs. 1 and 3A). The similarity in the dominant modal size between riverbed sands of Liangzi River and dune sands indicates that dune sands may have been reworked and sorted by the Liangzi River when the river expanded (Figs. 1 and 3A). The coarse 'tail' of aeolian sands has similar modal size to dune sands (Fig. 3A), indicating that these aeolian sands may have been sourced from dune sands. Nevertheless, the grain-size characteristics of these potential source materials differ significantly from those of the surface sediments from nearshore, transitional and offshore zones of the lake (Fig. 3B), supporting the inference that the clastic sediments in the lake are strongly reworked and sorted within the water body at present.

The grain-size distributions of clastic deposits with a single component should exhibit a unimodal, symmetrical distribution on a logarithmic scale, representing a single sedimentary process and

depositional environment (Ashley, 1978). When the shape of a grain-size distribution is asymmetrical or skewed, the total distribution could be considered as a combination of several unimodal distributions, representing several different patterns of transportation or different depositional environments (Ashley, 1978). Deep sea sediments consist of a dominant long-term suspension clay component (modal size: 2–3 μm) representing aeolian deposition and a suspension fine-silt component (modal size: 12–18 μm) representing hemipelagic input or volcanic ash (Rea et al., 1985; Rea and Hovan, 1995). Fluvial deposits are composed mainly of a saltation medium-sand component (modal size: 200–400 μm) and a suspension fine-silt component (modal size: 10–15 μm) (Middleton, 1976; Ashley, 1978; Bennett and Best, 1995). Typical loess deposits consist of a dominant short-term suspension medium-to-coarse silt component (modal size: 16–32 μm) and a long-term suspension clay-to-fine silt component (modal size: 2–6 μm) (Pye, 1987; Tsoar and Pye, 1987; Sun et al., 2002; Qin et al., 2005), whereas desert sands consist of a dominant saltation fine-to-medium sand component (modal size: 100–200 μm) and a suspension clay-to-fine silt component (modal size: 2–6 μm) (Gillette et al., 1974; Pye, 1987; Tsoar and Pye, 1987). The log-normal distribution function fitting results of multimodal grain-size distributions of surface sediments from Dali Lake (Xiao et al., 2015) and Hulun Lake (Xiao et al., 2012) exhibit five to six distinct unimodal distributions related to their specific hydraulic dynamics during the depositional processes. Components C1–C6

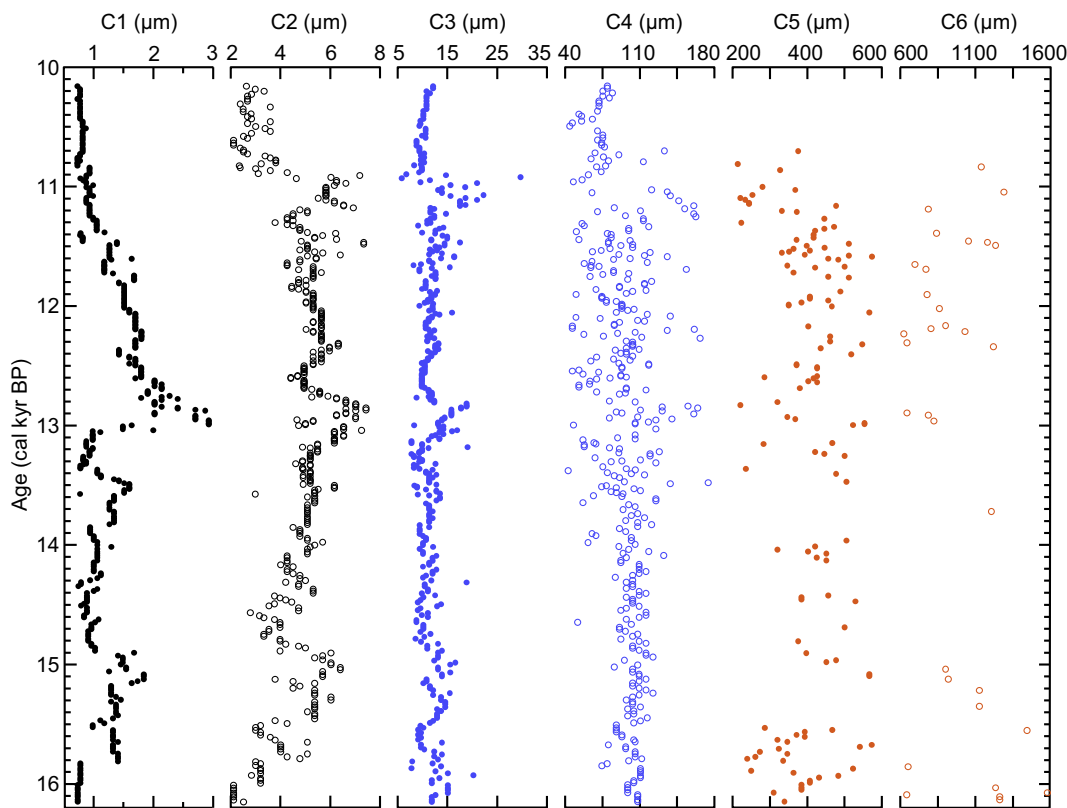


Fig. 4. Time series of modal sizes of components C1–C6 for the interval 7.71–11.83 m (16.2–10 cal kyr BP) of core DL04.

Table 2

Characteristic of the six grain-size components recognized in the polymodal distributions of samples from the interval 7.71–11.83 m of core DL04.

Component	Number of samples	Modal size (µm)		Percentage (%)	
		Min.	Max.	Min.	Max.
C1	413	0.8	3.0	0.5	23.3
C2	413	2.2	7.5	1.3	87.0
C3	413	6.2	30.2	2.0	82.5
C4	362	41.6	172.8	0.3	69.8
C5	125	210.1	570.9	0.3	60.3
C6	32	603.7	1568.1	0.5	15.5

respectively represent, from fine to coarse modes, long-term suspension clay, offshore-suspension fine silt, offshore-suspension medium to coarse silt, nearshore-suspension fine sand, nearshore-saltation medium sand and nearshore-traction coarse sand (Xiao et al., 2012, 2015). The relatively narrow ranges of the modal sizes of components C3 and C4 in the core sediments from Dali Lake (Fig. 4; Table 2) likely reflect minor fluctuations in the vigor of hydrodynamic processes within their specific depositional environments, and the discrete ranges of these two components (Fig. 4; Table 2) further supports the conclusion that they represent two distinct sets of hydraulic conditions, offshore and nearshore suspension, respectively. In addition, the nearshore zone of the lake basin is very steep, and the lake center is very flat (Fig. 1). Such a topography of the lake basin may have caused the abrupt transition of hydrological dynamics from nearshore to offshore zones, and thus the absence or insignificance of transitional component.

Hydraulic conditions in lakes are related to basin morphometry (water depth, size and shape) and the surrounding relief (Håkanson and Jansson, 1983; Sly, 1989a, 1989b). The shallow water of the nearshore zone generally possesses higher energy than the offshore zone, and therefore the sediment grain size decreases with increasing water depth (Håkanson and Jansson, 1983; Sly, 1989a, 1989b). Dali Lake is the

second largest lake in Inner Mongolia, and the location of core DL04 is about 5 km from the nearest shoreline (Fig. 1). When the lake level was lower, the distance between the core location and the lakeshore would have decreased, resulting in the increased representation of the nearshore grain-size components (C4, C5 and C6) at the core site. Thus, increases in the percentages of these nearshore components can be used to indicate decreases in lake level, which is demonstrated by the significant negative correlation between the percentages of components C4, C5 and C6 in the surface sediments from Dali Lake and Hulun Lake and water depth (Xiao et al., 2012, 2015). In addition, the nearshore components may also occur in sediments from the offshore zone (such as component C4 in sample a10 in Fig. 3B). These relatively coarse particles in the deep-water zone may represent aeolian sands, blown by strong winds, which was trapped on the frozen lake surface and then supplied to the water column after thawing of the ice (Xiao et al., 2012). However, this component is unlikely to dominate the grain-size distribution of the sediments in the offshore zone (Fig. 3B), due to the predominance of hydrodynamic processes in this large lake at present.

The prevailing winds in the Dali Lake catchment are northwesterly and westerly winds in spring and winter when dust storms are frequent (Wang et al., 2002). The lake basin sits at the northern margin of the Hunshandake Sandy Lands (Fig. 1). Hills of basaltic rocks surround the lake to the north and west (Li, 1993). Therefore aeolian activity should not play an important role in the sediment supply for Dali Lake at present. The Asian dust export during the Holocene was probably related to the intensity of the northwesterly winds (Xu et al., 2018). During the early to middle Holocene, strong East Asian winter monsoon (EAWM) (Fig. 1) caused high dust accumulation in the downwind areas including the northern China (Xu et al., 2018); while the nearshore components C4 and C5 in the Dali Lake sediments during this period reached the lowest values through the entire Holocene (Xiao et al., 2015). These data imply that aeolian dust could not have made a large contribution to the components C4 and C5 in Dali Lake during the Holocene. On the contrary, high percentages of the nearshore

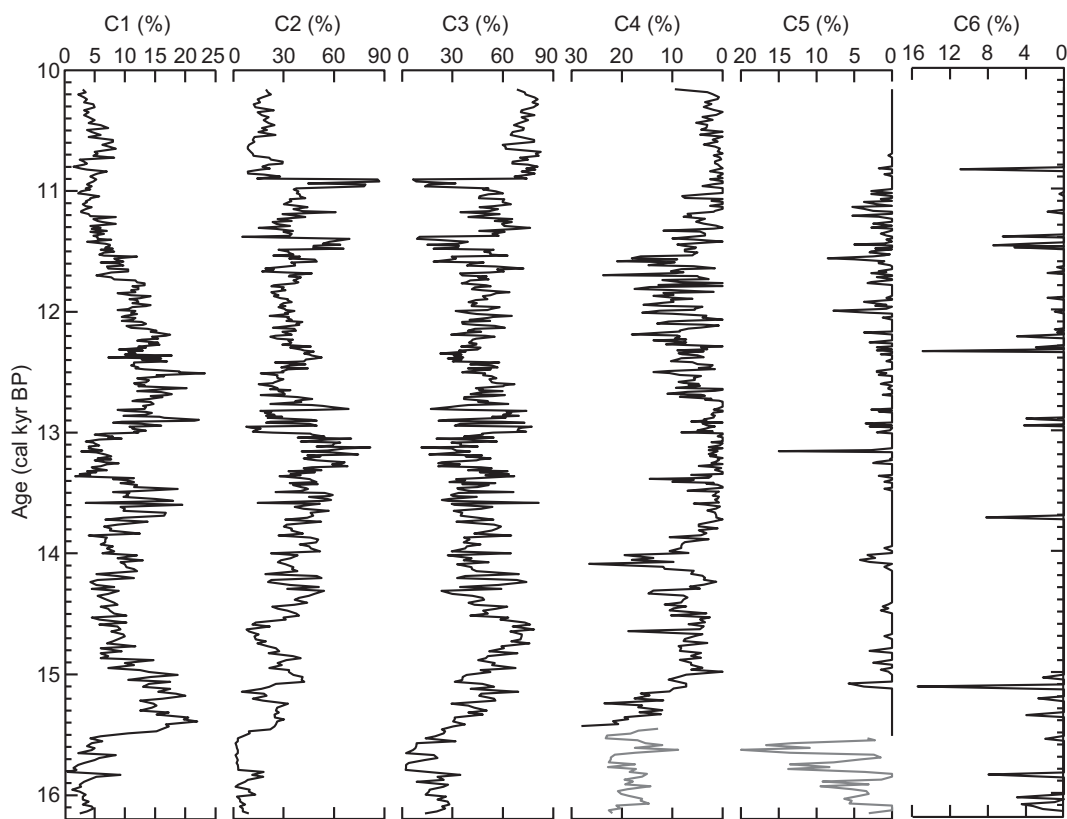


Fig. 5. Time series of percentages of components C1–C6 for the interval 7.71–11.83 m (16.2–10 cal kyr BP) of core DL04. The grey solid line represents 1/3 of the original values.

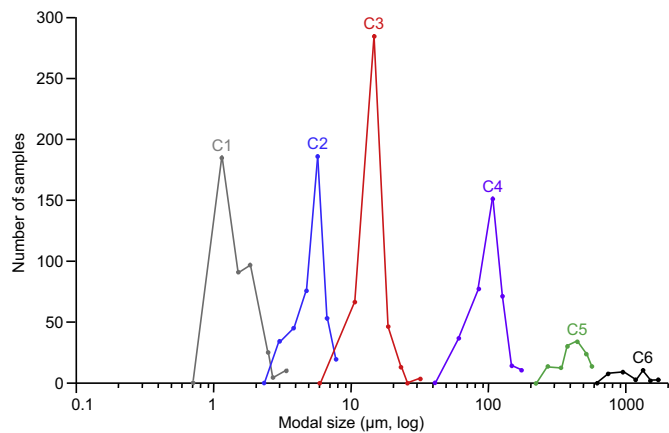


Fig. 6. Frequency of the modal sizes of the six grain-size components, C1–C6, within the 413 samples from the interval 7.71–11.83 m (16.2–10 cal kyr BP) of core DL04.

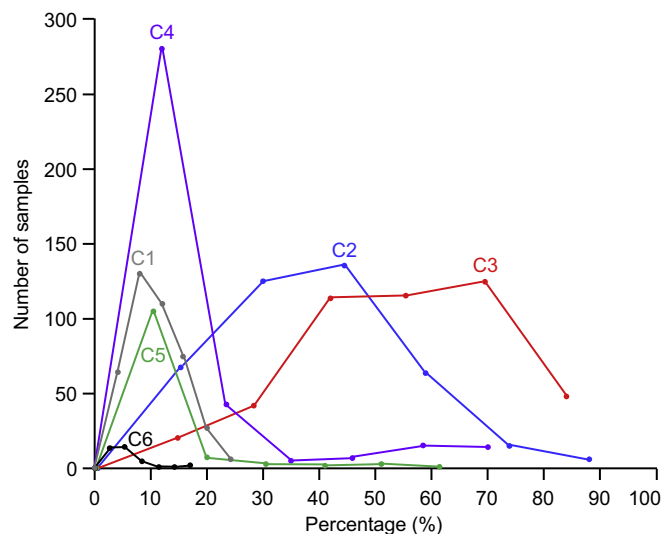


Fig. 7. Frequency of the percentages of the six grain-size components, C1–C6, within the 413 samples from the interval 7.71–11.83 m (16.2–10 cal kyr BP) of core DL04.

components C4 and C5 in Dali Lake correlated well with low regional precipitation reconstructed from pollen assemblages during the Holocene (Xiao et al., 2012, 2015), supporting that high percentages of the nearshore components (C4 + C5) should reflect a lowered lake level during the Holocene.

While compared with the Holocene grain-size data of Dali Lake (Xiao et al., 2015), the deglacial data exhibit a unique coarse component C6 (Figs. 4 and 5; Table 2). In addition, the modal sizes of component C5 are also much larger during the last deglaciation (210.1–570.9 µm) than during the Holocene (203.0–514.7 µm) (Xiao et al., 2015) (Fig. 4; Table 2). These data may indicate that the deglacial condition was significantly different from the Holocene. Previous studies on the initiation and variation of the Hunshandake Sandy Lands

(Fig. 1) suggested that the areas of the sandy lands during the last deglaciation should be much larger than during the Holocene, due to the deglacial drier climate and less vegetation cover in the region (Yang et al., 2013). The sandy lands may have expanded northward, surrounding the lake to the west and east during the last deglaciation. The nearshore zone of the lake at present may have also been partially exposed at that time. Therefore a part of the coarse components in the Dali Lake sediments may have also been sourced from the sandy lands and the exposed shoreline materials transported by strong aeolian

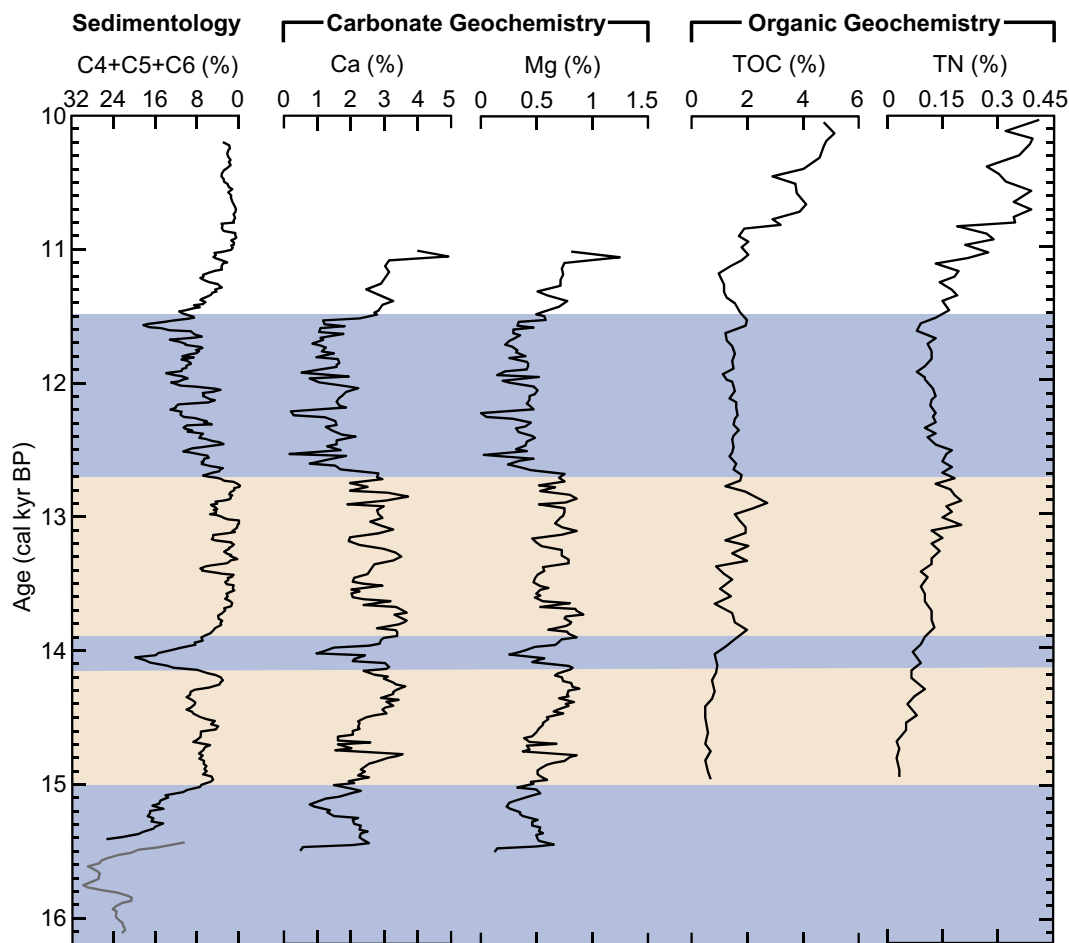


Fig. 8. Correlation of the percentage of components C4, C5 and C6 from 413 samples from the interval 7.71–11.83 m (16.2–10 cal kyr BP) of core DL04 with Ca and Mg concentrations in < 38- μ m calcites (Fan et al., 2018b), and total organic carbon (TOC) and total nitrogen (TN) concentrations (Fan et al., 2017) from the same sediment core. The percentages of components C4, C5 and C6 are smoothed using a 5-point moving average. The grey solid line represents 1/3 of the original values.

activities during the last deglaciation. Anyway, the significant increases in the percentage of these coarse components should have been attributed to both strong aeolian activities and low lake levels during the last deglaciation. Although dust emission by strong aeolian activities may have been closely related to sand supply, vegetation cover and wind strength or atmospheric circulation (Qiang et al., 2014), the coincidence between strong aeolian activities and low lake levels would indicate a common factor controlling them, that is the dry climate in the region. Therefore high percentages of the coarse components (C4 + C5 + C6) could indicate drought events in the region.

5.2. Droughts in the Dali Lake region

The high-resolution time series of the percentage of the coarse components (C4 + C5 + C6) from 16.2–10 cal kyr BP indicate that drought events occurred during 16.2–15 and 12.7–11.5 cal kyr BP (Fig. 8). The period of 15–12.7 cal kyr BP is characterized by generally wet climate, although an interval of significantly dry climate occurred during 14.15–13.9 cal kyr BP (Fig. 8). The regional climate was relatively wet after 11.5 cal kyr BP (Fig. 8).

Recent studies on the carbonate geochemistry of the Dali Lake sediments suggest that the < 38- μ m calcites in the sediments are dominated by endogenic calcites precipitated within the lake water (Fan et al., 2016, 2018b). The precipitation of calcites in the lake water depends on the balance between ionic activity product (IAP) of Ca^{2+} and CO_3^{2-} and the equilibrium constant K_c (Lerman, 1978). The Ca^{2+} in the lake water is mainly controlled by strong evaporation in brackish

lakes such as Dali Lake (Fan et al., 2016). The CO_3^{2-} in the lake water is mainly controlled by the dissolved CO_2 concentration which is closely related to the lake water temperature and the biological activities (Liu et al., 2014; Chen et al., 2016). The K_c is mainly controlled by the temperature (Lerman, 1978). Dali Lake is located in the semi-arid areas, and Ca^{2+} and CO_3^{2-} in the lake water are preferentially precipitated as calcite when evaporation intensifies and dissolved CO_2 concentration decreases, both of which should be mainly controlled by increases in regional temperature during the last deglaciation when biological productivity was generally low and varied in small amplitudes (Fan et al., 2017). Mg^{2+} in the lake water is progressively incorporated into calcite when $\text{Mg}^{2+}/\text{Ca}^{2+}$ ratio gradually increases (Fan et al., 2016). Therefore increases in the Ca and Mg concentrations of the endogenic calcites in Dali Lake could indicate increases in regional temperature, and vice versa (Fan et al., 2018b). The drought events suggested by the high percentages of the coarse components (C4 + C5 + C6) generally correspond with low regional temperatures at 15–12.7 and 12.7–11.5 cal kyr BP on millennial timescales (Fig. 8). In addition, the regional climate was significantly dry at the interval 14.15–13.9 cal kyr BP, therefore the synchronous low values of Ca and Mg concentrations should also indicate low regional temperatures during this time (Fig. 8). However, Ca and Mg concentrations were high at 15.5–15 cal kyr BP when the lake levels were low (Fig. 8), indicating that drying climate may have dominated the precipitation of calcites during this interval.

In addition, the total organic carbon (TOC) and total nitrogen (TN) concentrations of the Dali Lake sediments could reflect the hydrological status and the ecology of the lake catchment (Fan et al., 2017). High

sedimentary TOC and TN concentrations should indicate increased terrestrial organic matter and nutrient inputs to the lake and enhanced organic productivity within the catchment related to increases in regional temperature and precipitation (Fan et al., 2017). The drought events indicated by the high percentages of the coarse components (C4 + C5 + C6) in sediment core DL04 are generally consistent with the low regional precipitation and temperature indicated by the low TOC and TN concentrations in the same core at 13.9–12.7 and 12.7–11.5 cal kyr BP on millennial timescales (Fig. 8). However, in this semi-arid area at the northern margin of the EASM, the response of the ecological status of the lake catchment to regional climatic change may not be as sensitive as the hydrological status (Fan et al., 2017). For example, when regional climate was relatively wet at 15–14.15 cal kyr BP, the TOC and TN concentrations exhibited low values (Fig. 8) during this interval. The growth of vegetation in the lake catchment should be closely related to the degree of soil development. During the transition from the interval 16.2–15 to 15–14.15 cal kyr BP, the hydrological conditions should have been improved while the soil may have not been developed, resulting in lagged or insensitive response of ecological status to climatic change.

5.3. Possible mechanisms of the droughts in northern China

The overall consistency between the sedimentological, carbonate and organic geochemical characteristics of the Dali Lake sediments (Fig. 8), which to some degree reflect independent processes operating within the lake catchment, together with their respective paleoenvironmental implications, implies that the drought events were likely related to a significantly weakened EASM intensity, which resulted in synchronous decreases in regional precipitation and temperature.

A weakened EASM intensity in northern China during 16.2–15 and 12.7–11.5, as well as during 14.15–13.9 cal kyr BP, is supported by coeval decreases in summer temperature inferred from a record of long-chain alkenones from the sediments of Sihailongwan Lake (Sun et al., 2018b), and by decreases in regional humidity reconstructed from pollen assemblages from Moon Lake (Wu et al., 2016) and Gonghai Lake (Chen et al., 2015a) (Figs. 1 and 9). Although the environmental implications of the oxygen isotope record of stalagmites is debated (Maher, 2008; Tan, 2014; Fan et al., 2018a), the precise dating of stalagmites has made it a benchmark for paleoclimatic comparisons. The present study highlights the occurrence of centennial-scale drought conditions during 14.15–13.9 cal kyr BP, and the oxygen isotope record of stalagmites from Hulu Cave clearly records this event (Wang et al., 2001) (Fig. 9). The coherent response of the two proxies highlights the paleoclimatic significance of this event.

The high-resolution record of droughts at the modern northern margin of the EASM indicate that the EASM intensity weakened significantly during 16.2–15 and 12.7–11.5 cal kyr BP; these events may correspond, within the age uncertainties, to the millennial-scale Heinrich 1 (H1) and Younger Dryas (YD) events occurring in the North Atlantic and Northern European region. The events were well recorded by the oxygen isotope record from Greenland ice cores (e.g., NGRIP) (Buiertz et al., 2014) (Fig. 9). It was suggested that the significantly reduced formation of North Atlantic Deep Water (NADW), possibly triggered by a large amount of high northern latitude meltwater input to the North Atlantic (Tarasov and Peltier, 2005), caused significant temperature decreases in the North Atlantic and Northern European region during the intervals of H1 and YD (Johnsen et al., 2001). Geological records and numerical modeling results both suggest that the intensification of the circumpolar circulation due to cooling over northern high latitudes could have suppressed the northward penetration of the EASM circulation on millennial timescales (Sun et al., 2012; Tan et al., 2018). Several studies also suggest that the southwestward migration of the West Pacific subtropical high (WPSH), related to the increased amplitude and frequency of the El Niño-Southern Oscillation (ENSO), would have increased monsoonal precipitation in the middle

reaches of the Yangtze River at the interval corresponding to the YD (Huang et al., 2012; Xie et al., 2013). In addition, it has been argued that ENSO variability could have played the dominant role in increasing the monsoonal precipitation in northeast China during this interval, through regulating the intensity and position of the WPSH (Hong et al., 2010). They suggested that the occurrence of an El Niño-like phenomenon would cause a northward movement of the WPSH and monsoonal rain-belt towards the northern China (Hong et al., 2010). Although it is still heatedly debated on the relationship between the WPSH and ENSO variability (Wang and Chen, 2012), such a low latitude forcing suggested by Hong et al. (2010) should have had limited influence on climatic change in the Dali Lake region during this interval when the region experienced significant drought (Fig. 9).

The significant drought on centennial timescales recorded by the grain-size record of Dali Lake occurred at 14.15–13.9 cal kyr BP, and it may correspond to the prominent cold reversal, the Older Dryas (OD) event in the North Atlantic and Northern European region (Fig. 9). The ^{14}C age uncertainties at 14.15 and 13.9 cal kyr BP are from -314 to 285 and from -297 to 241 yr, respectively (Fig. 9), which indicates that this centennial-scale drought could not have occurred before 14.435 cal kyr BP ($14,150 + 285$ yr) and after 13.603 cal kyr BP ($13,900 - 297$ yr), based on the Bayesian age–depth model (Fig. 2). This leads us to conclude that there was a causal relationship between this significant drought event and the OD cold climatic reversal (Fig. 9). Such a centennial-scale climatic event is recorded in monsoonal Asia (e.g., Wang et al., 2001; Nakagawa et al., 2005; Stebich et al., 2009; Park et al., 2014; Gorbarenko et al., 2017; Sun et al., 2018b) or in the Asia interior (e.g., Prokopenko et al., 1999) at middle to high latitudes. For example, the alkenone-inferred temperature record from the varved sediments of Sihailongwan Lake indicates a summer temperature decrease of $3\text{--}5\text{ }^{\circ}\text{C}$ in northeastern China at 14.3–13.9 cal kyr BP (Sun et al., 2018b); and the absolutely-dated stalagmite oxygen isotope record from Hulu Cave in eastern China shows a positive shift during 14.2–13.9 cal kyr BP (Wang et al., 2001), which was likely related to a weakened EASM intensity based on multi-proxy comparison, although the amplitude was much smaller than those in Dali and Sihailongwan Lake (Fig. 9); however, there is virtually no clear evidence for such a centennial-scale event in southeastern China. The likely decreasing response of the EASM to the OD cold reversal, from northern to southern China, suggests that the climatic change signal propagated between high and low latitudes was mainly via atmospheric transmission rather than by oceanic circulation (Fan et al., 2017, 2018b).

The grain-size data from the Dali Lake sediments clearly record both millennial- and centennial-scale droughts at the EASM margin during the last deglaciation. These droughts can be recognized as responses to cold climatic reversals occurring at northern high latitudes, probably via a mechanism of atmospheric coupling between high and middle latitudes. Furthermore, our data imply that even a small decrease in high-latitude temperature (e.g., the OD reversal during the BA warm phase) could result in a significantly weakened EASM intensity and thus lead to drought in the semi-arid areas of northern China. The cold reversals associated with Arctic ice expansion and reduction in Atlantic Meridional Overturning Circulation (AMOC) across northern high latitudes were induced by the rapid input of glacial melt-water during the global climatic warming of the last deglaciation. Since past climatic warming may have caused droughts in northern China via high-latitude ice-sheet melting, careful consideration should be given to the implications of continued greenhouse gas emissions and consequent global climatic warming. Actually, both sea surface temperature (SST) observations (Caesar et al., 2018) and numerical model results (Thornalley et al., 2018) have already provided the evidence for a weakening of the AMOC over the past 150 yr. The results may indicate that global warming could cause high-latitude cooling through ice-sheet melting at present, which would then lower the temperature of north-westerly and westerly winds over East Asia, deliver cold air masses to northern China (Zheng et al., 2017), eventually resulting in significant

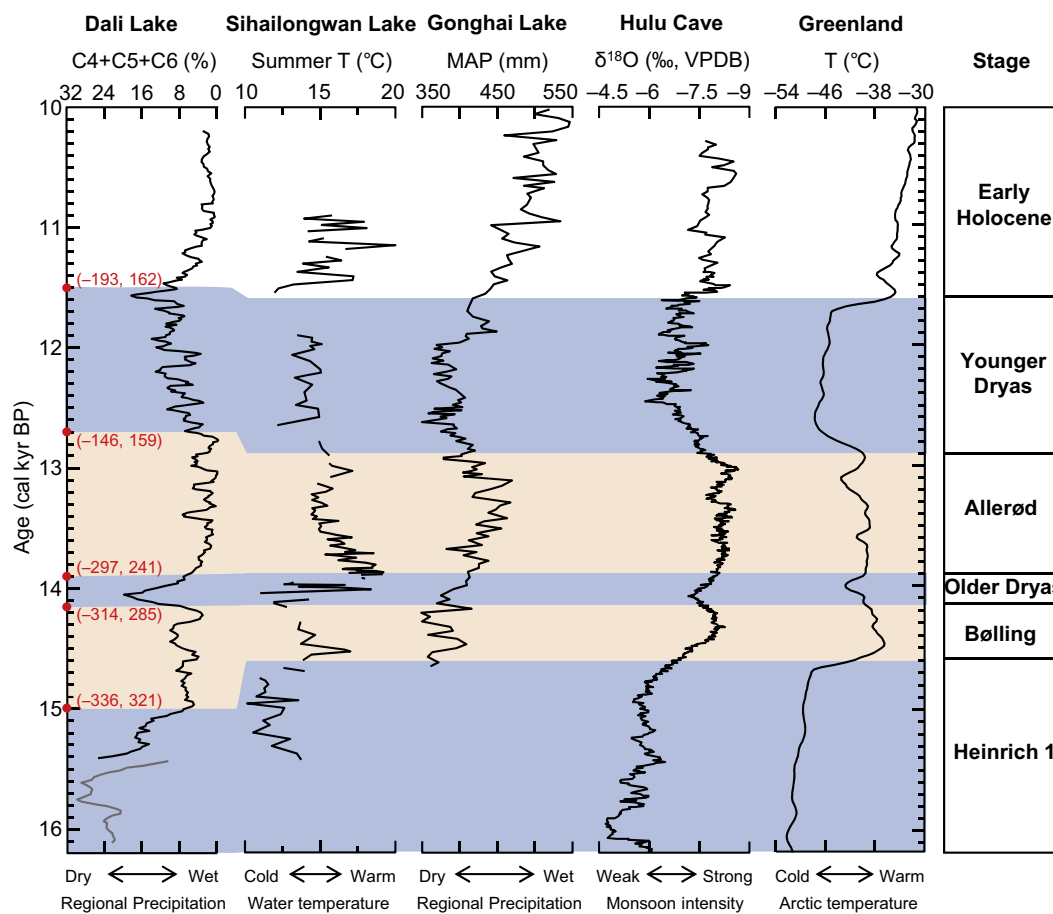


Fig. 9. Correlation of the percentage of components C4, C5 and C6 from 413 samples from the interval 7.71–11.83 m (16.2–10 cal kyr BP) of core DL04 with summer temperature inferred from the long-chain alkenone record from Sihailongwan Lake (Sun et al., 2018b), mean annual precipitation (MAP) reconstructed from pollen assemblages at Gonghai Lake (Chen et al., 2015a), $\delta^{18}\text{O}$ record of stalagmites from Hulu Cave (Wang et al., 2001), and the $\delta^{15}\text{N}$ -based temperature record from Greenland (Buizert et al., 2014). The percentages of components C4, C5 and C6 are smoothed using a 5-point moving average. The grey solid line represents 1/3 of the original values. The red solid circles represent the calibrated ^{14}C dates based on the age–depth model (see Fig. 2) and the numbers in brackets indicate the ranges of uncertainties. (For interpretation of the references to colour in this figure legend, the reader is referred to the web version of this article.)

weakening in the EASM intensity and thus drought in northern China.

6. Conclusions

The clastic sediments of Dali Lake generally comprise fluvial material and aeolian dust during the last deglaciation. The grain-size distributions of the Dali Lake sediments are partitioned using a specific log-normal distribution function fitting method. High percentages of the coarse components (C4 + C5 + C6) indicate strong aeolian activities and low lake levels, and thus droughts in the region. The drought events are accompanied by decreases in regional temperature, catchment surface runoff and bio-productivity. These findings imply that the northern margin of the East Asian summer monsoon (EASM) experienced significantly weakened EASM intensity. In addition, the drought events may be linked, within the age uncertainties, to the Heinrich 1 (H1) and Younger Dryas (YD) events on millennial timescales, and to the Older Dryas (OD) event on centennial timescales. This suggests the occurrence of strong high-latitude forcing, probably via an atmospheric coupling between high and middle latitudes. These cold reversals over northern high latitudes were induced by the rapid influx of glacial meltwater to the North Atlantic during the last deglaciation. Hence, the possible implications of ongoing anthropogenic climatic warming, and resulting high-latitude ice-sheet melting, for the increased occurrence of droughts in northern China should be carefully considered.

Acknowledgments

The corresponding author is grateful to Prof. Dr. Ruilin Wen, Drs. Shengrui Zhang and Yun Huang for helpful discussions. We would like to extend our sincere thanks to Prof. Dr. Paul Hesse and two anonymous reviewers for their constructive comments and suggestions on the original version of this manuscript, and thank Prof. Dr. Jan Bloemendal for English polishing. This study is supported by the Strategic Priority Research Program of Chinese Academy of Sciences (grant XDB26000000), National Key Research and Development Program of China (grant 2017YFA0603400), National Natural Science Foundation of China (grants 41702179, 41130101 and 41672166) and the China Postdoctoral Science Foundation (grants 2018T110138 and 2017M610111).

References

- An, Z.S., 2000. The history and variability of the East Asian paleomonsoon climate. *Quat. Sci. Rev.* 19, 171–187.
- Ashley, G.M., 1978. Interpretation of polymodal sediments. *J. Geol.* 86, 411–421.
- Bennett, S.J., Best, J.L., 1995. Mean flow and turbulence structure over fixed, two dimensional dunes: implications for sediment transport and bedform stability. *Sedimentology* 42, 491–513.
- Blaauw, M., Christen, J.A., 2011. Flexible paleoclimate age–depth models using an autoregressive gamma process. *Bayesian Anal.* 6, 457–474.
- Bronk Ramsey, C., Lee, S., 2013. Recent and planned developments of the program OxCal. *Radiocarbon* 55, 720–730.
- Buizert, C., Gkinis, V., Severinghaus, J.P., He, F., Lecavalier, B.S., Kindler, P.,

- Leuenberger, M., Carlson, A.E., Vinther, B., Masson-Delmotte, V., White, J.W.C., Liu, Z.Y., Otto-Bliesner, B., Brook, E.J., 2014. Greenland temperature response to climate forcing during the last deglaciation. *Science* 345, 1177–1180.
- Caesar, L., Rahmstorf, S., Robinson, A., Feulner, G., Saba, V., 2018. Observed fingerprint of a weakening Atlantic Ocean overturning circulation. *Nature* 556, 191–196.
- Chen, F.H., Xu, Q.H., Chen, J.H., Birks, H.J.B., Liu, J.B., Zhang, S.R., Jin, L.Y., An, C.B., Telford, R.J., Cao, X.Y., Wang, Z.L., Zhang, X.J., Selvaraj, K., Lu, H.Y., Li, Y.C., Zheng, Z., Wang, H.P., Zhou, A.F., Dong, G.H., Zhang, J.W., Huang, X.Z., Bloemendal, J., Rao, Z.G., 2015a. East Asian summer monsoon precipitation variability since the last deglaciation. *Sci. Rep.* 5, 11186. <https://doi.org/10.1038/srep11186>.
- Chen, J.H., Chen, F.H., Feng, S., Huang, W., Liu, J.B., Zhou, A.F., 2015b. Hydroclimatic changes in China and surroundings during the medieval climate anomaly and little ice age: spatial patterns and possible mechanisms. *Quat. Sci. Rev.* 107, 98–111.
- Chen, F.H., Wu, D., Chen, J.H., et al., 2016. Holocene moisture and East Asian summer monsoon evolution in the northeastern Tibetan Plateau recorded by Lake Qinghai and its environs: a review of conflicting proxies. *Quat. Sci. Rev.* 154, 111–129.
- Cheng, H., Edwards, R.L., Sinha, A., Spötl, C., Yi, L., Chen, S.T., Kelly, M., Kathayat, G., Wang, X.F., Li, X.L., Kong, X.G., Wang, Y.J., Ning, Y.F., Zhang, H.W., 2016. The Asian monsoon over the past 640,000 years and ice age terminations. *Nature* 534, 640–646.
- Chu, G.Q., Sun, Q., Zhu, Q.Z., Shan, Y.B., Shang, W.Y., Ling, Y., Su, Y.L., Xie, M.M., Wang, X.S., Liu, J.Q., 2017. The role of the Asian winter monsoon in the rapid propagation of abrupt climate changes during the last deglaciation. *Quat. Sci. Rev.* 177, 120–129.
- Compilatory Commission of Vegetation of China, 1980. *Vegetation of China*. Science Press, Beijing, pp. 932–955 (in Chinese).
- Ding, Y.H., Wang, Z.Y., Sun, Y., 2008. Inter-decadal variation of the summer precipitation in East China and its association with decreasing Asian summer monsoon. Part I: observed evidences. *Int. J. Climatol.* 28, 1139–1161.
- Fan, J.W., Xiao, J.L., Wen, R.L., Zhang, S.R., Wang, X., Cui, L.L., Li, H., Xue, D.S., Yamagata, H., 2016. Droughts in the East Asian summer monsoon margin during the last 6 kyr: link to the North Atlantic cooling events. *Quat. Sci. Rev.* 151, 88–99.
- Fan, J.W., Xiao, J.L., Wen, R.L., Zhang, S.R., Wang, X., Cui, L.L., Yamagata, H., 2017. Organic geochemical investigations of the Dali Lake sediments: implications for environment and climate changes of the last deglaciation in the East Asian summer monsoon margin. *J. Asian Earth Sci.* 140, 135–146.
- Fan, J.W., Xiao, J.L., Wen, R.L., Zhang, S.R., Huang, Y., Yue, J.J., Wang, X., Cui, L.L., Li, H., Xue, D.S., Liu, Y.H., 2018a. Mineralogy and carbonate geochemistry of the Dali Lake sediments: implications for paleohydrological changes in the East Asian summer monsoon margin during the Holocene. *Quat. Int.* <https://doi.org/10.1016/j.quaint.2018.03.019>. in press.
- Fan, J.W., Xiao, J.L., Wen, R.L., Zhang, S.R., Wang, X., Cui, L.L., Liu, Y.H., Li, H., Yue, J.J., 2018b. The manifestation of the Younger Dryas event in the East Asian summer monsoon margin: new evidence from carbonate geochemistry of the Dali Lake sediments in northern China. *The Holocene* 28, 1082–1092.
- Gillette, D.A., Blifford, D.A., Fryer, D.W., 1974. The influence of wind velocity on size distributions of soil wind aerosols. *J. Geophys. Res.* 79, 4068–4075.
- Gorbarenko, S.A., Shi, X.F., Malakhova, G.Y., Bosin, A.A., Zou, J.J., Liu, Y.G., Chen, M.-T., 2017. Centennial to millennial climate variability in the far northwestern Pacific (off Kamchatka) and its linkage to the East Asian monsoon and North Atlantic from the Last Glacial Maximum to the early Holocene. *Clim. Past* 13, 1063–1080.
- Håkanson, L., Jansson, M., 1983. *Principles of Lake Sedimentology*. Springer, Berlin (316 pp).
- Hong, B., Hong, Y.T., Lin, Q.H., Shibata, Y., Uchida, M., Zhu, Y.X., Leng, X.T., Wang, Y., Cai, C.C., 2010. Anti-phase oscillation of Asian monsoons during the Younger Dryas period: evidence from peat cellulose $\delta^{13}\text{C}$ of Hani, Northeast China. *Palaeogeogr. Palaeoclimatol. Palaeoecol.* 297, 214–222.
- Huang, X.Y., Meyers, P.A., Yu, J.X., Wang, X.X., Huang, J.H., Jin, F., Gu, Y.S., Xie, S.C., 2012. Moisture conditions during the Younger Dryas and the early Holocene in the middle reaches of the Yangtze River, central China. *The Holocene* 22, 1473–1479.
- Huang, C., Wei, G.J., Li, W.X., Liu, Y., 2018. A geochemical record of the link between chemical weathering and the East Asian summer monsoon during the late Holocene preserved in lacustrine sediments from Poyang Lake, central China. *J. Asian Earth Sci.* 154, 17–25.
- Johnsen, S.J., Dahl-Jensen, D., Gundestrup, N., Steffensen, J.P., Clausen, H.B., Miller, H., Masson-Delmotte, V., Sveinbjörnsdóttir, A.E., White, J., 2001. Oxygen isotope and palaeotemperature records from six Greenland ice-core stations: Camp Century, Dye-3, GRIP, GISP2, Renland and North GRIP. *J. Quat. Sci.* 16, 299–307.
- Lerman, A., 1978. *Lakes: Chemistry, Geology, Physics*. Springer, pp. 363.
- Li, Z.G., 1993. *Annals of Hexigten Banner*. People's Press of Inner Mongolia, Hohhot (1144 pp in Chinese).
- Liu, X.J., Colman, S.M., Brown, E.T., et al., 2014. Abrupt deglaciation on the northeastern Tibetan Plateau: evidence from Lake Qinghai. *J. Paleolimnol.* 51, 223–240.
- Lu, F.Z., Ma, C.M., Zhu, C., Lu, H.Y., Zhang, X.J., Huang, K.Y., Guo, T.H., Li, K.F., Li, L., Li, B., Zhang, W.Q., 2018. Variability of East Asian summer monsoon precipitation during the Holocene and possible forcing mechanisms. *Clim. Dyn.* <https://doi.org/10.1007/s00382-018-4175-6>. in press.
- Maher, B.A., 2008. Holocene variability of the East Asian summer monsoon from Chinese cave records: a re-assessment. *The Holocene* 18, 861–866.
- Middleton, G.V., 1976. Hydraulic interpretation of sand size distributions. *J. Geol.* 84, 405–426.
- Nakagawa, T., Kitagawa, H., Yasuda, Y., Tarasov, P.E., Gotanda, K., Sawai, Y., 2005. Pollen/event stratigraphy of the varved sediment of Lake Suigetsu, central Japan from 15,701 to 10,217 SG vyr BP (Suigetsu varve years before present): description, interpretation, and correlation with other regions. *Quat. Sci. Rev.* 24, 1691–1701.
- Park, J., Lim, H.S., Lim, J., Park, Y.-H., 2014. High-resolution multi-proxy evidence for millennial- and centennial-scale climate oscillations during the last deglaciation in Jeju Island, South Korea. *Quat. Sci. Rev.* 105, 112–125.
- Prokopenko, A.A., Williams, D.F., Karabanov, E.B., Khursevich, G.K., 1999. Response of Lake Baikal ecosystem to climate forcing and pCO_2 change over the last glacial/interglacial transition. *Earth Planet. Sci. Lett.* 172, 239–253.
- Pye, K., 1987. *Aeolian Dust and Dust Deposits*. Academic Press, pp. 29–62.
- Qiang, M.R., Liu, Y.Y., Jin, Y.X., Song, L., Huang, X.T., Chen, F.H., 2014. Holocene record of eolian activity from Genggahai Lake, northeastern Qinghai-Tibetan Plateau, China. *Geophys. Res. Lett.* 41, 589–595. <https://doi.org/10.1002/2013GL058806>.
- Qin, X.G., Cai, B.G., Liu, T.S., 2005. Loess record of the aerodynamic environment in the east Asia monsoon area since 60,000 years before present. *J. Geophys. Res.* 110, B01204. <https://doi.org/10.1029/2004JB003131>.
- Rao, Z.G., Li, Y.X., Zhang, J.W., Jia, G.D., Chen, F.H., 2016. Investigating the long-term palaeoclimatic controls on the δD and $\delta^{18}\text{O}$ of precipitation during the Holocene in the Indian and East Asian monsoonal regions. *Earth Sci. Rev.* 159, 292–305.
- Rea, D.K., Hovan, S.A., 1995. Grain size distribution and depositional processes of the mineral component of abyssal sediments: lessons from the North Pacific. *Paleoceanography* 10, 251–258.
- Rea, D.K., Leinen, M., Janecek, T.R., 1985. Geologic approach to the long-term history of atmospheric circulation. *Science* 227, 721–725.
- Reimer, P.J., Bard, E., Bayliss, A., Beck, J.W., Blackwell, P.G., Bronk Ramsey, C., Buck, C.E., Cheng, H., Edwards, R.L., Friedrich, M., Grootes, P.M., Guilderson, T.P., Hafliðason, H., Hajdas, I., Hatté, C., Heaton, T.J., Hoffmann, D.L., Hogg, A.G., Hughen, K.A., Kaiser, K.F., Kromer, B., Manning, S.W., Niu, M., Reimer, R.W., Richards, D.A., Scott, E.M., Southon, J.R., Staff, R.A., Turney, C.S.M., van der Plicht, J., 2013. INTCAL13 and MARINE13 radiocarbon age calibration curves, 0–50,000 years cal BP. *Radiocarbon* 55, 1869–1887.
- Russell, J.M., Vogel, H., Konecky, B.L., Bijaksana, S., Huang, Y.S., Melles, M., Wattrus, N., Costa, K., King, J.W., 2014. Glacial forcing of central Indonesian hydroclimate since 60,000 y B.P. *Proc. Natl. Acad. Sci.* 111, 5100–5105.
- Sly, P.G., 1989a. Sediment dispersion: part 1, fine sediments and significance of the silt/clay ratio. *Hydrobiologia* 176 (177), 99–110.
- Sly, P.G., 1989b. Sediment dispersion: part 2, characterization by size of sand fraction and percent mud. *Hydrobiologia* 176 (177), 111–124.
- Stebich, M., Mingram, J., Han, J.T., Liu, J.Q., 2009. Late Pleistocene spread of (cool-) temperate forests in Northeast China and climate changes synchronous with the North Atlantic region. *Glob. Planet. Chang.* 65, 56–70.
- Stebich, M., Mingram, J., Moschen, R., Thiele, A., Schröder, C., 2011. Comments on “Anti-phase oscillation of Asian monsoons during the younger dryas period: evidence from peat cellulose $\delta^{13}\text{C}$ of Hani, Northeast China” by B. Hong, Y.T. Hong, Q.H. Lin, Yasuyuki Shibata, Masao Uchida, Y.X. Zhu, X.T. Leng, Y. Wang and C.C. Cai [Palaeogeography, Palaeoclimatology, Palaeoecology 297 (2010) 214–222]. *Palaeogeogr. Palaeoclimatol. Palaeoecol.* 310, 464–470.
- Sun, D.H., Bloemendal, J., Rea, D.K., Vandenberghe, J., Jiang, F.C., An, Z.S., Su, R.X., 2002. Grain-size distribution function of polymodal sediments in hydraulic and aeolian environments, and numerical partitioning of the sedimentary components. *Sediment. Geol.* 152, 263–277.
- Sun, Y.B., Steven, C.C., Morrill, C., Lin, X.P., Wang, X.L., An, Z.S., 2012. Influence of Atlantic meridional overturning circulation on the East Asian winter monsoon. *Nat. Geosci.* 5, 46–49.
- Sun, Q., Chu, G.Q., Xie, M.M., Zhu, Q.Z., Su, Y.L., Wang, X.S., 2018a. An oxygen isotope record from Lake Xiarinur in Inner Mongolia since the last deglaciation and its implication for tropical monsoon change. *Glob. Planet. Chang.* 163, 109–117.
- Sun, Q., Chu, G.Q., Xie, M.M., Ling, Y., Su, Y.L., Zhu, Q.Z., Shan, Y.B., Liu, J.Q., 2018b. Long-chain alkenone-inferred temperatures from the last deglaciation to the early Holocene recorded by annually laminated sediments of the maar lake Sihailongwan, northeastern China. *The Holocene* 28, 1173–1180.
- Tan, M., 2014. Circulation effect: response of precipitation $\delta^{18}\text{O}$ to the ENSO cycle in monsoon regions of China. *Clim. Dyn.* 42, 1067–1077.
- Tan, L.C., Cai, Y.J., Cheng, H., Edwards, L.R., Gao, Y.L., Xu, H., Zhang, H.W., An, Z.S., 2018. Centennial- to decadal-scale monsoon precipitation variations in the upper Hanjiang River region, China over the past 6650 years. *Earth Planet. Sci. Lett.* 482, 580–590.
- Tarasov, L., Peltier, W.R., 2005. Arctic freshwater forcing of the Younger Dryas cold reversal. *Nature* 435, 662–665.
- Thornalley, D.J.R., Oppo, D.W., Ortega, P., Robson, J.I., Brierley, C.M., Davis, R., Hall, I.R., Moffa-Sanchez, P., Rose, N.L., Spooner, P.T., Yashayev, I., Keigwin, L.D., 2018. Anomalously weak Labrador Sea convection and Atlantic overturning during the past 150 years. *Nature* 556, 227–230.
- Tsoar, H., Pye, K., 1987. Dust transport and the question of desert loess formation. *Sedimentology* 34, 139–153.
- Wang, H.J., Chen, H.P., 2012. Climate control for southeastern China moisture and precipitation: Indian or East Asian monsoon? *J. Geophys. Res.* 117, D12109. <https://doi.org/10.1029/2012JD017734>.
- Wang, Y.J., Cheng, H., Edwards, R.L., An, Z.S., Wu, J.Y., Shen, C.-C., Dorale, J.A., 2001. A high-resolution absolute-dated late Pleistocene monsoon record from Hulu Cave, China. *Science* 294, 2345–2348.
- Wang, G.L., Lv, D.R., You, L., 2002. Analyses of climatic characteristics on Hunshandake dust storm. *Climatic Environ. Res.* 7, 433–439 (in Chinese with English abstract).
- Wang, Y.J., Cheng, H., Edwards, R.L., He, Y.Q., Kong, X.G., An, Z.S., Wu, J.Y., Kelly, M.J., Dykoski, C.A., Li, X.D., 2005. The Holocene Asian monsoon: links to solar changes and North Atlantic climate. *Science* 308, 854–857.
- Wang, X.S., Chu, G.Q., Sheng, M., Zhang, S.Q., Li, J.H., Chen, Y., Tang, L., Su, Y.L., Pei, J.L., Yang, Z.Y., 2016. Millennial-scale Asian summer monsoon variations in South China since the last deglaciation. *Earth Planet. Sci. Lett.* 451, 22–30.
- Wen, R.L., Xiao, J.L., Fan, J.W., Zhang, S., Yamagata, H., 2017. Pollen evidence for a mid-Holocene East Asian summer monsoon maximum in northern China. *Quat. Sci. Rev.* 176, 29–35.

- Wu, J., Liu, Q., Wang, L., Chu, G.Q., Liu, J.Q., 2016. Vegetation and climate change during the last deglaciation in the Great Khingan Mountain, Northeastern China. *PLoS One* 11 (1), e0146261. <https://doi.org/10.1371/journal.pone.0146261>.
- Xiao, J.L., Xu, Q.H., Nakamura, T., Yang, X.L., Liang, W.D., Inouchi, Y., 2004. Holocene vegetation variation in the Daihai Lake region of north-central China: a direct indication of the Asian monsoon climatic history. *Quat. Sci. Rev.* 23, 1669–1679.
- Xiao, J.L., Si, B., Zhai, D.Y., Itoh, S., Lomtadze, Z., 2008. Hydrology of Dali Lake in central-eastern Inner Mongolia and Holocene East Asian monsoon variability. *J. Paleolimnol.* 40, 519–528.
- Xiao, J.L., Chang, Z.G., Fan, J.W., Zhou, L., Zhai, D.Y., Wen, R.L., Qin, X.G., 2012. The link between grain-size components and depositional processes in a modern clastic lake. *Sedimentology* 59, 1050–1062.
- Xiao, J.L., Fan, J.W., Zhai, D.Y., Wen, R.L., Qin, X.G., 2015. Testing the model for linking grain-size component to lake level status of modern clastic lakes. *Quat. Int.* 355, 34–43.
- Xie, S.C., Evershed, R.P., Huang, X.Y., Zhu, Z.M., Pancost, R.D., Meyers, P.A., Gong, L.F., Hu, C.Y., Huang, J.H., Zhang, S.L., Gu, Y.S., Zhu, J.Y., 2013. Concordant monsoon-driven postglacial hydrological changes in peat and stalagmite records and their impacts on prehistoric cultures in central China. *Geology* 41, 827–830.
- Xu, B., Wang, L., Gu, Z.Y., Hao, Q.Z., Wang, H.Z., Chu, G.Q., Jiang, D.B., Liu, Q., Qin, X.G., 2018. Decoupling of climatic drying and Asian dust export during the Holocene. *J. Geophys. Res. Atmos.* 123. <https://doi.org/10.1002/2017JD027483>.
- Yan, H., Sun, L.G., Oppo, D.W., Wang, Y.H., Liu, Z.H., Xie, Z.Q., Liu, X.D., Cheng, W.H., 2011. South China Sea hydrological changes and Pacific Walker Circulation variations over the last millennium. *Nat. Commun.* 2, 293. <https://doi.org/10.1038/ncomms1297>.
- Yang, X.P., Wang, X.L., Liu, Z.T., Li, H.W., Ren, X.Z., Zhang, D.G., Ma, Z.B., Rioual, P., Jin, X.D., Scuderi, L., 2013. Initiation and variation of the dune fields in semi-arid China—with a special reference to the Hunshandake Sandy Land, Inner Mongolia. *Quat. Sci. Rev.* 78, 369–380.
- Zheng, Y.H., Pancost, R.D., Liu, X.D., Wang, Z.Z., Naafs, B.D.A., Xie, X.X., Liu, Z., Yu, X.F., Yang, H., 2017. Atmospheric connections with the North Atlantic enhanced the glacial warming in northeast China. *Geology* 45, 1031–1034.
- Zhong, W., Wei, Z.Q., Shang, S.T., Ye, S.S., Tang, X.W., Zhu, C., Xue, J.B., Ouyang, J., Smol, J.P., 2018. A 15,400-year record of environmental magnetic variations in sub-alpine lake sediments from the western Nanling Mountains in South China: Implications for palaeoenvironmental changes. *J. Asian Earth Sci.* 154, 82–92.
- Zhou, X., Sun, L.G., Chu, Y.X., Xia, Z.H., Zhou, X.Y., Li, X.Z., Chu, Z.D., Liu, X.J., Shao, D., Wang, Y.H., 2016. Catastrophic drought in East Asian monsoon region during Heinrich event 1. *Quat. Sci. Rev.* 141, 1–8.